Electronic Supplementary Information (ESI)

Atomic-scale mechanisms on stepwise growth of $Mo_xW_{1-x}S_2$ into hexagonal flakes

Jiawei Huang,[a] Zhouyang Zhang,[a] Yiran Ying,[b] Min Gan,[a] Haitao Huang[b] and Linfeng Fei*[a]

[a] School of Physics and Materials Science, Nanchang University, Nanchang, Jiangxi 330031, China

[b] Department of Applied Physics and Research Institute for Smart Energy, The Hong Kong Polytechnic University, Kowloon, Hong Kong, China

E-mail: feilinfeng@gmail.com (L.F.)

Contents of Supplementary Information:

1. Experimental section

1-1. TGA/DSC measurement

Simultaneous TGA/DSC analysis were carried out using a STA449 F5 instrument. A 10 mg sample of $(NH_4)_2MoS_4$ or $(NH_4)_2WS_4$ powder was transferred to an alumina crucible and heated to 800 ^oC with a constant ramping rate of 20 ^oC min^{-1} under N_2 flow (100 mL min^{-1}).

1-2. Preparation of TEM specimen

High purity of $(NH_4)_2MoS_4$ and $(NH_4)_2WS_4$ were dissolved in N, N-dimethylformamide (DMF) in a 1:1 molar ratio to form a 1 wt% precursor solution, which was sonicated for 20 min. The TEM sample was prepared by drop-casting the precursor solution on a Si_3N_4 membrane supported by a silicon E-Chip, which was then naturally dried in air.

1-3. In situ TEM observations

In situ TEM experiments in this work were performed with a DENSsolutions Wildfire heating holder. TEM experiments were conducted on a JEOL JEM-F200 cold-field-emission TEM operated at 200 kV equipped with an EDS detector. TEM images were recorded using a Gatan OneView IS camera with an optimized exposure time. For TEM heating experiments, sample was first heated within the TEM from RT to 100 ^oC with a ramping rate of 5 ^oC s^{-1}. The temperature was maintained at 100 ^oC for 30 min to remove any possible organic residues. Subsequently, the sample was heated from 100 to 1100 ^oC in 50 ^oC increments with a ramping rate of 5 ^oC s^{-1}. After each 50 ^oC increment, the sample temperature was held for 30 min during TEM imaging. Noteworthy, the beam valve was closed after each particular heating step to minimize the electron beam effects. During the TEM observations, the sample was irradiated with an electron dose rate of ≈5000 e^- $Å^{-2}$ s^{-1}. To monitor the influence of electron beam irradiation on the growth dynamics, we compared the observed area with the places not exposed to the e-beam after every heating step. The detailed procedure and results are described in Fig. S15.

1-4. Computational details

Density functional theory (DFT) calculations were performed within the projector augmented-wave scheme implemented in VASP code.[1,2] Perdew-Burke-Ernzerhof generalized gradient approximation was used for the exchange-correlation functional.[3] DFT-D3 method was used for the van der Waals correction.[4] Kinetic energy cutoff was set as 450 eV, and energy/force convergence criteria were set as 10^{-5} eV and 0.02 eV $Å^{-1}$, respectively. A 5×5 Monkhorst-Pack k-points mesh was used to sample the first Brillouin zone for the four-layer 2×2 supercell of MS_2 (M=Mo/W). The four structures of MoS_2/WS_2 solid solution were constructed by randomly replacing half of the Mo atoms with W in MoS_2. A vacuum layer with the thickness of more than 15 Å was used to avoid spurious interactions between adjacent layers.

2. Supporting figures

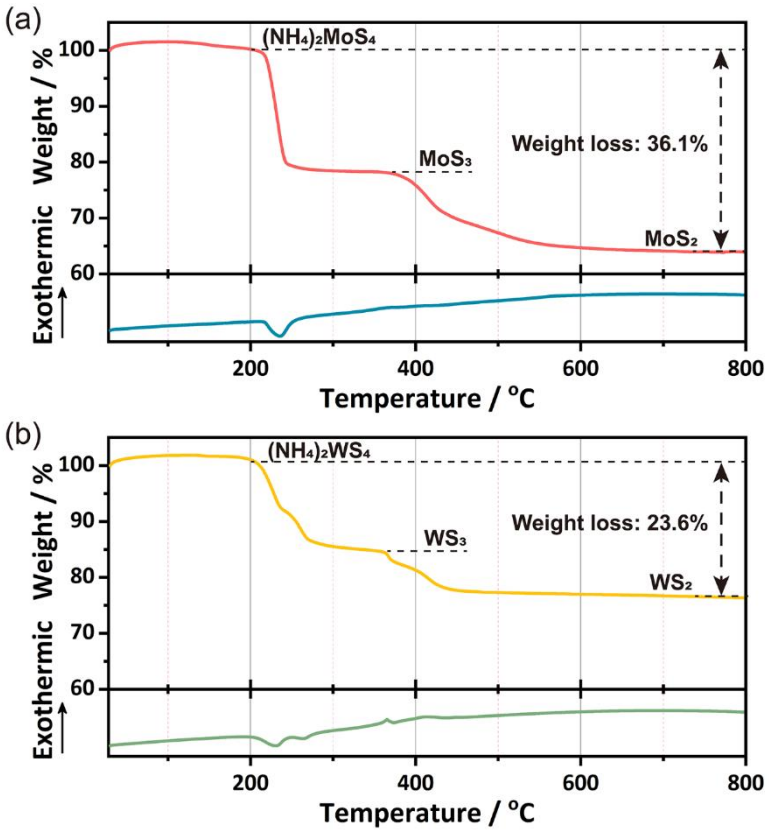

Fig. S1 TG-DSC profiles for $(NH_4)_2MoS_4$ and $(NH_4)_2WS_4$ precursors. The profiles suggest that $(NH_4)_2MoS_4$ in (a) and $(NH_4)_2WS_4$ in (b) both undergo two steps of thermal decomposition; $(NH_4)_2MoS_4$ transforms to MoS_2 with a weight loss of 38.5% and $(NH_4)_2WS_4$ transforms to WS_2 with a weight loss of 23.6%.

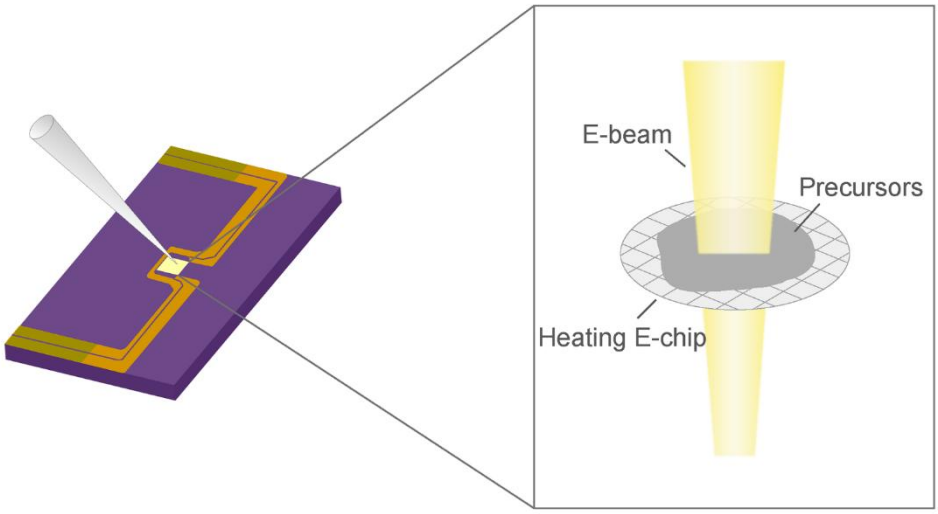

Fig. S2 An illustration of our experimental design. The precursor solution was drop-casted onto the heating chip, and was then heated and observed inside TEM after drying.

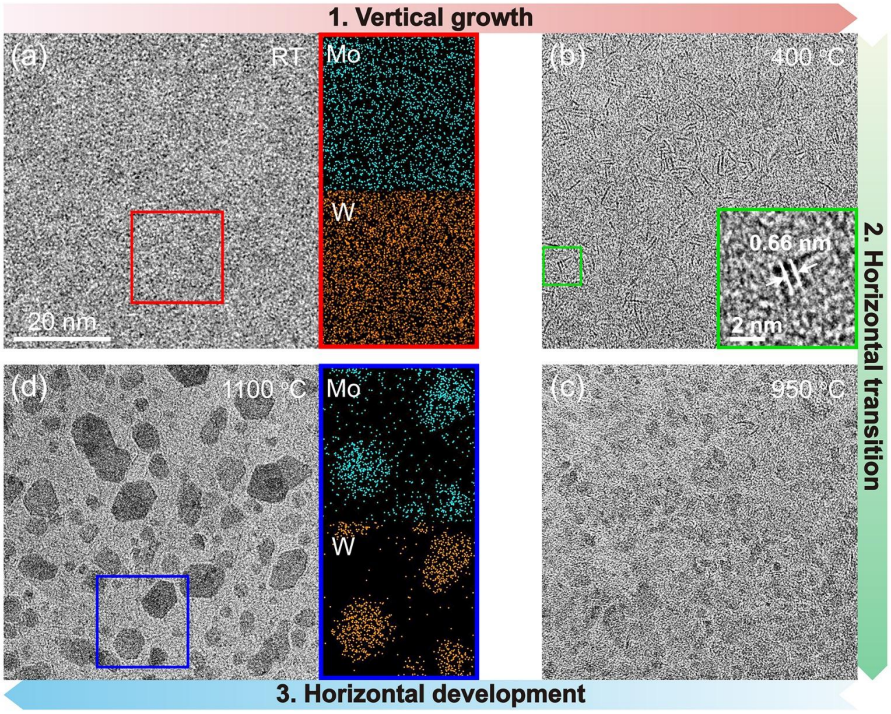

Fig. S3 (a) TEM image of the amorphous precursor. (b-d) The in situ TEM image series shows the temperature-induced morphological changes of precursor. The insets in (a, d) include the elemental mappings for Mo and W, which were respectively obtained from the regions delimited by the red/blue boxes. The bottom-right inset in (b) shows a high-magnification view of a three-layer vertical $Mo_xW_{1-x}S_2$. The scale bar in (a) also applies to (b-d).

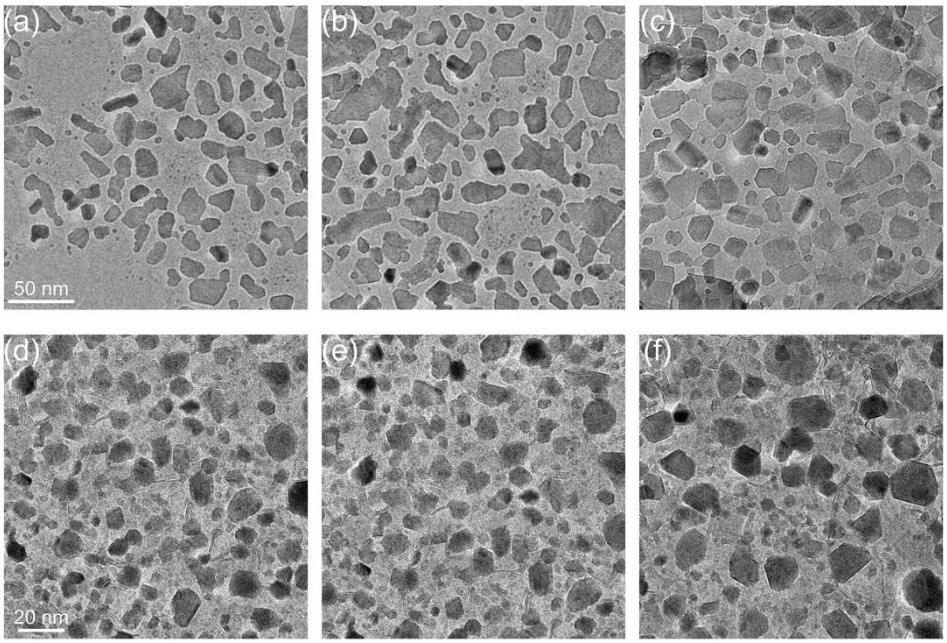

Fig. S4 Observation of MoS_2 and WS_2 flakes under low magnification TEM. (a)-(c) TEM images for MoS_2 decomposed form $(NH_4)_2MoS_4$ precursor heating to 1000 ^oC. (d)-(f) TEM images for WS_2 decomposed form $(NH_4)_2WS_4$ precursor heating to 1000 ^oC. Hexagonal MoS_2 or WS_2 flakes are barely observed. The scale bar in (a) also applies to (b, c), and the scale bar in (d) also applies to (e, f).

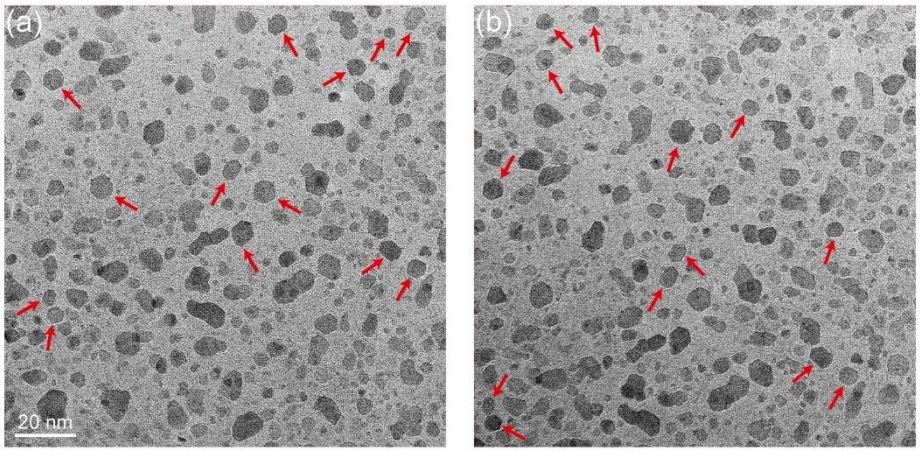

Fig. S5 Observation of hexagonal $Mo_xW_{1-x}S_2$ flakes under low magnification TEM. The red arrows in (a) and (b) are used to highlight the hexagonal flakes. The scale bar in (a) also applies to (b).

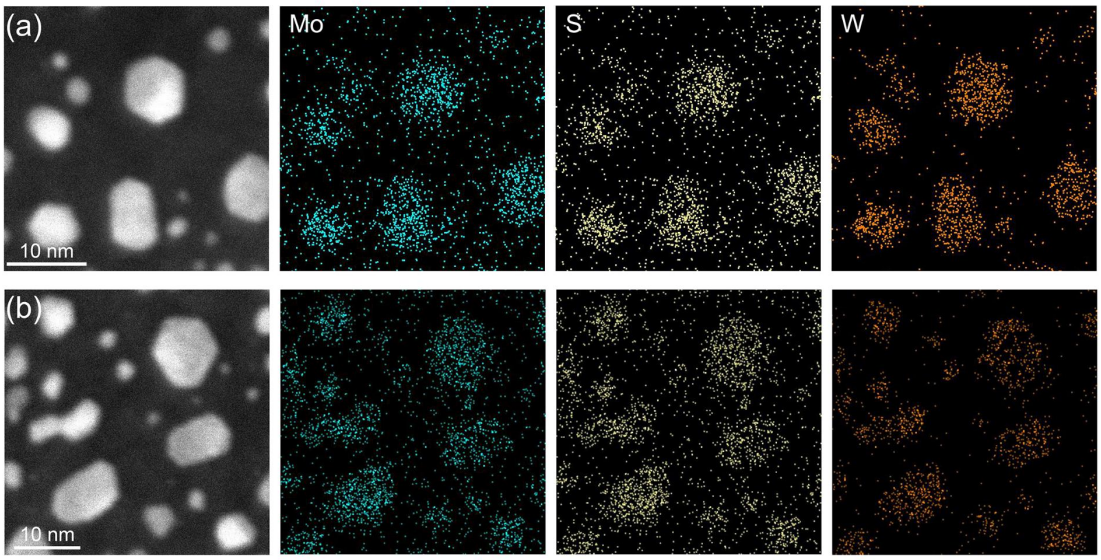

	Mo (mol%)	W (mol%)	S (mol%)
a	24.7	13.5	61.8
b	22.1	14.6	63.3

Fig. S6 Elemental analysis for the hexagonal flakes of $Mo_xW_{1-x}S_2$ alloy after cooling to RT. (a)-(b) The STEM images of two imaged regions and the corresponding elemental mapping of Mo, S and W, respectively. The mol ratios of Mo, W and S of these two sets of elemental mappings are also provided in the table below.

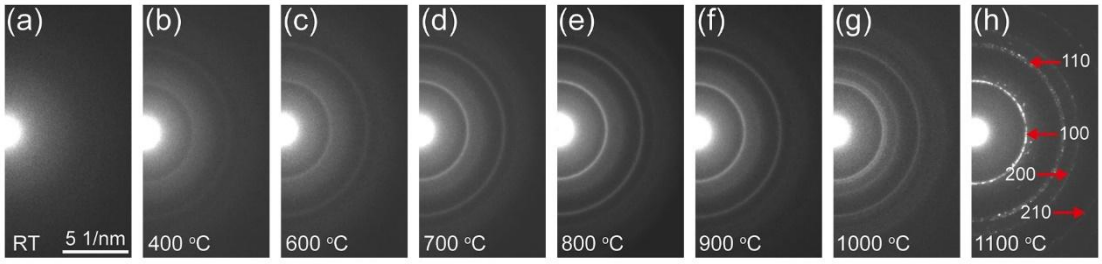

Fig. S7 Evolution of SAED patterns from in situ experiments. (a)-(h) The SADE patterns obtained from RT to 1100 °C. The diffraction rings belonging to $Mo_xW_{1-x}S_2$ alloy are shown in (h). The scale bar in (a) also applies to (b-h).

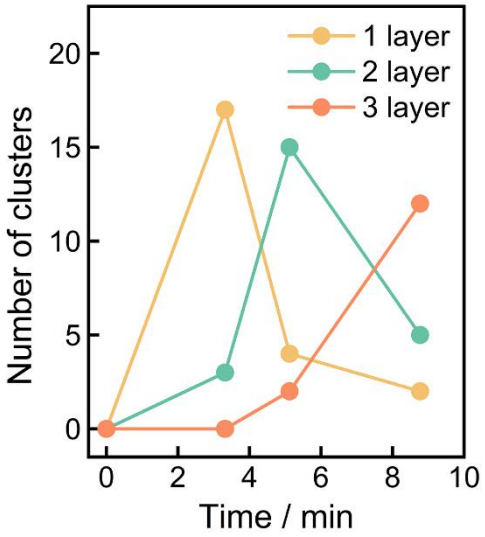

Fig. S8 The change of number of vertical clusters with 1, 2 and 3 layer(s) in Fig. 2 (a-d) as a function of time.

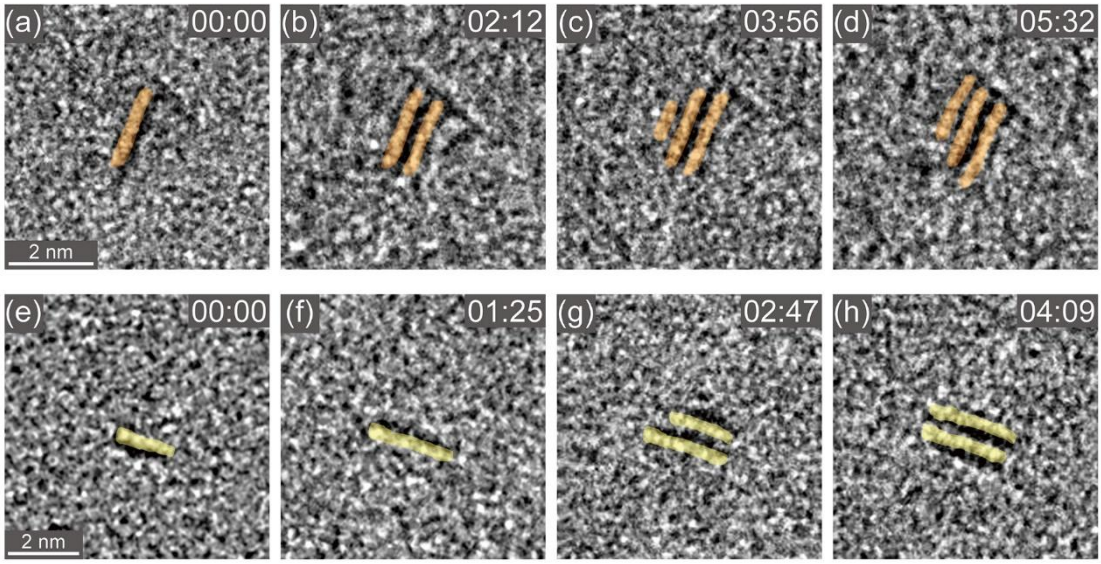

Fig. S9 In situ TEM images of the layer-by-layer growth of vertical $Mo_xW_{1-x}S_2$ at 400 ºC. Coloured sketches are included to illustrate the $Mo_xW_{1-x}S_2$ layers. The scale bar in (a) also applies to (b-d), and the scale bar in (e) also applies to (f-h).

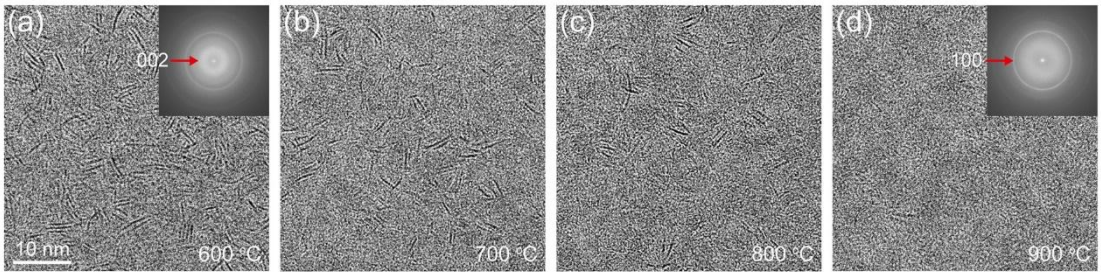

Fig. S10 TEM images showing the vertical-to-horizontal transition versus temperature for $Mo_xW_{1-x}S_2$. The insets in (a) and (d) are the corresponding fast Fourier transform (FFT) patterns. The scale bar in (a) also applies to (b-d).

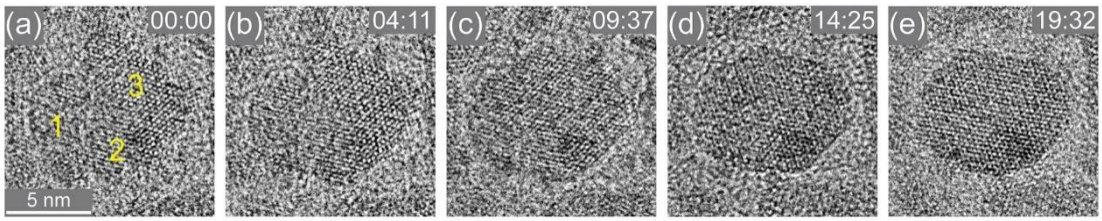

Fig. S11 In situ TEM images of assembly and the subsequent development of $Mo_xW_{1-x}S_2$ flakes at 950 °C. The scale bar in (a) also applies to (b-e).

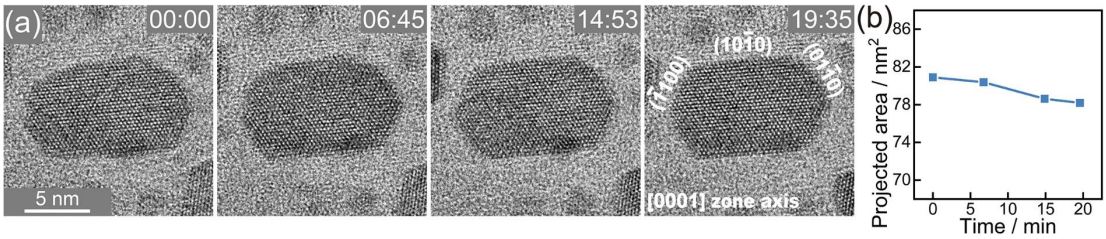

Fig. S12 Formation of an elongated hexagonal $Mo_xW_{1-x}S_2$ flake at 1050 °C. (a) In situ TEM images on growth of an elongated hexagonal flake. (b) The corresponding plot for projected area of the flake in (a) as a function of time.

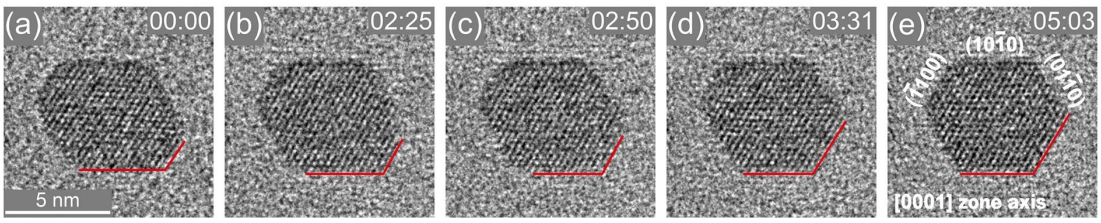

Fig. S13 Evolution of $Mo_xW_{1-x}S_2$ structure into hexagonal flake at 1100 °C. Red lines in (a)-(e) are included to emphasize the edges. The scale bar in (a) also applies to (b-e).

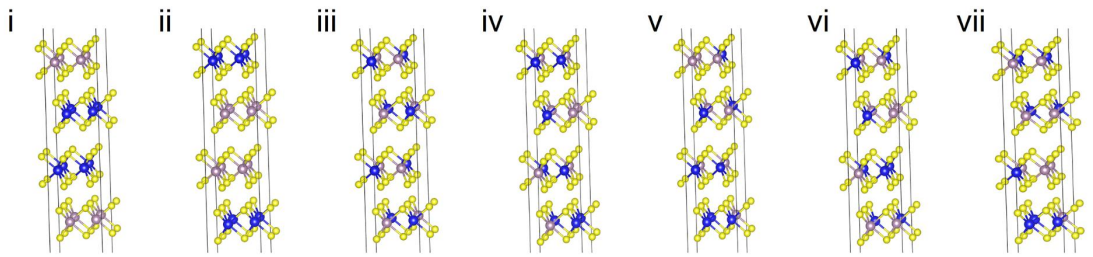

Fig. S14 Optimized structures of four-layer 2×2 supercell structures of MS_2 with the atomic ratio Mo: W=1:1. Color code: Mo, purple; W, blue; S, yellow.

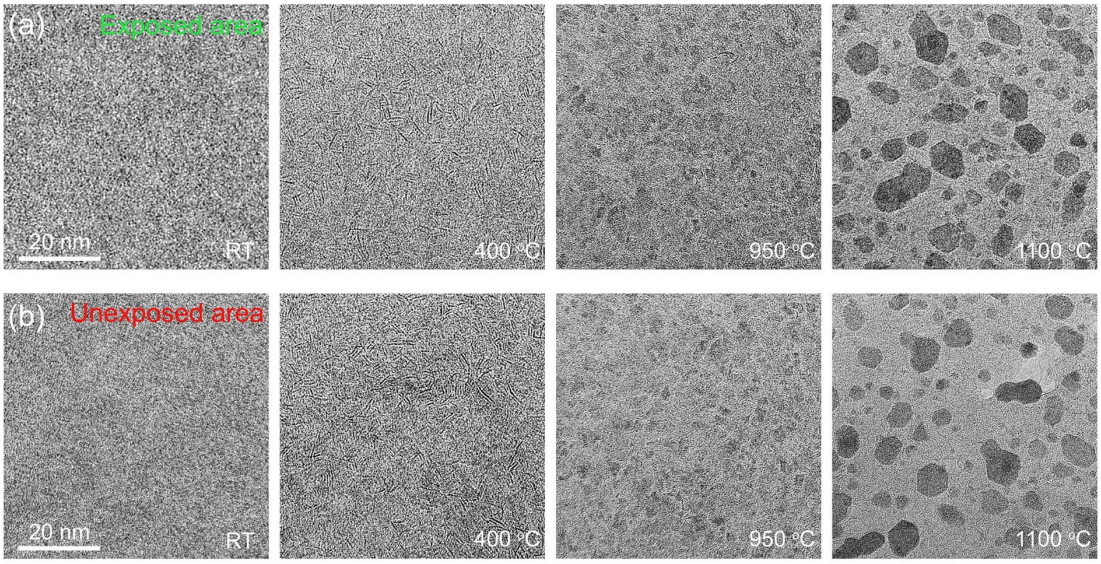

Fig. S15 Investigation on the effect of electron beam irradiation on the growth dynamics. The stepwise evolution of $Mo_xW_{1-x}S_2$ into hexagonal flakes at an exposed area (a) and an unexposed area (b), respectively.

References

[1] G. Kresse and J. Furthmüller, *Phys. Rev. B* 1996, **54**, 11169-11186.

[2] G. Kresse and D. Joubert, *Phys. Rev. B* 1999, **59**, 1758-1775.

[3] J. P. Perdew, K. Burke and M. Ernzerhof, *Phys. Rev. Lett.*, 1996, **77**, 3865-3868.

[4] S. Grimme, J. Antony, S. Ehrlich and H. Krieg, *J. Chem. Phys.*, 2010, **132**, 154104.